arXiv:2304.06967v1 [astro-ph.HE] 14 Apr 2023

X-ray polarization evidence for a 200 years-old flare of Sgr A*

Frédéric Marin[1], Eugene Churazov[2,3], Ildar
Khabibullin[4,2,3], Riccardo Ferrazzoli[5], Laura
Di Gesu[6], Thibault Barnouin[1], Alessandro Di
Marco[5], Riccardo Middei[7,8], Alexey Vikhlinin[9,3], Enrico
Costa[5], Paolo Soffitta[5], Fabio Muleri[5], Rashid
Sunyaev[2,3], William Forman[9], Ralph Kraft[9], Stefano
Bianchi[10], Immacolata Donnarumma[6], Pierre-Olivier
Petrucci[11], Teruaki Enoto[12], Iván Agudo[13], Lucio A.
Antonelli[8,7], Matteo Bachetti[14], Luca Baldini[15,16], Wayne H.
Baumgartner[17], Ronaldo Bellazzini[15], Stephen D.
Bongiorno[17], Raffaella Bonino[18,19], Alessandro
Brez[15], Niccolò Bucciantini[20,21,22], Fiamma
Capitanio[5], Simone Castellano[15], Elisabetta
Cavazzuti[6], Chien-Ting Chen[23], Stefano
Ciprini[24,7], Alessandra De Rosa[5], Ettore Del Monte[5], Niccolò
Di Lalla[25], Victor Doroshenko[26], Michal Dovčiak[27], Steven R.
Ehlert[17], Yuri Evangelista[5], Sergio Fabiani[5], Javier A.
Garcia[28], Shuichi Gunji[29], Kiyoshi Hayashida[30], Jeremy
Heyl[31], Adam Ingram[32], Wataru Iwakiri[33,34], Svetlana G.
Jorstad[35,36], Philip Kaaret[17,37], Vladimir Karas[27], Takao
Kitaguchi[12], Jeffery J. Kolodziejczak[17], Henric
Krawczynski[38], Fabio La Monaca[5], Luca Latronico[18], Ioannis
Liodakis[39], Simone Maldera[18], Alberto Manfreda[15], Andrea
Marinucci[6], Alan P. Marscher[35], Herman L.
Marshall[40], Francesco Massaro[18,19], Giorgio Matt[10], Ikuyuki
Mitsuishi[41], Tsunefumi Mizuno[42], Michela Negro[43,44,45], C.-Y.
Ng[46], Stephen L. O'Dell[17], Nicola Omodei[25], Chiara
Oppedisano[18], Alessandro Papitto[8], George G. Pavlov[47], Abel
L. Peirson[25], Matteo Perri[7,8], Melissa Pesce-Rollins[15], Maura

Pilia[14], Andrea Possenti[14], Juri Poutanen[48], Simonetta Puccetti[7], Brian D. Ramsey[17], John Rankin[5], Ajay Ratheesh[5], Oliver J. Roberts[23], Roger W. Romani[25], Carmelo Sgrò[15], Patrick Slane[9], Gloria Spandre[15], Doug Swartz[23], Toru Tamagawa[12], Fabrizio Tavecchio[49], Roberto Taverna[50], Yuzuru Tawara[41], Allyn F. Tennant[17], Nicholas E. Thomas[17], Francesco Tombesi[51,24,52], Alessio Trois[14], Sergey S. Tsygankov[48], Roberto Turolla[50,53], Jacco Vink[54], Martin C. Weisskopf[17], Kinwah Wu[53], Fei Xie[55,5] and Silvia Zane[53]

¹Université de Strasbourg, CNRS, Observatoire Astronomique de Strasbourg, UMR 7550, 67000 Strasbourg, France.
²Max Planck Institute for Astrophysics, Karl-Schwarzschild-Strasse 1, 85741 Garching, Germany.
³Space Research Institute of the Russian Academy of Sciences, Profsoyuznaya Str. 84/32, Moscow 117997, Russia.
⁴Universitäts-Sternwarte, Fakultät für Physik, Ludwig-Maximilians-Universität München, Scheinerstr.1, 81679 München, Germany.
⁵INAF Istituto di Astrofisica e Planetologia Spaziali, Via del Fosso del Cavaliere 100, 00133 Roma, Italy.
⁶ASI - Agenzia Spaziale Italiana, Via del Politecnico snc, 00133 Roma, Italy.
⁷Space Science Data Center, Agenzia Spaziale Italiana, Via del Politecnico snc, 00133 Roma, Italy.
⁸INAF Osservatorio Astronomico di Roma, Via Frascati 33, 00078 Monte Porzio Catone (RM), Italy.
⁹Center for Astrophysics, Harvard & Smithsonian, 60 Garden St, Cambridge, MA 02138, USA.
¹⁰Dipartimento di Matematica e Fisica, Università degli Studi Roma Tre, Via della Vasca Navale 84, 00146 Roma, Italy.
¹¹Université Grenoble Alpes, CNRS, IPAG, 38000 Grenoble, France.
¹²RIKEN Cluster for Pioneering Research, 2-1 Hirosawa, Wako, Saitama 351-0198, Japan.
¹³Instituto de Astrofísica de Andalucía—CSIC, Glorieta de la Astronomía s/n, 18008 Granada, Spain.
¹⁴INAF Osservatorio Astronomico di Cagliari, Via della Scienza 5, 09047 Selargius (CA), Italy.

[15]Istituto Nazionale di Fisica Nucleare, Sezione di Pisa, Largo B. Pontecorvo 3, 56127 Pisa, Italy.

[16]Dipartimento di Fisica, Università di Pisa, Largo B. Pontecorvo 3, 56127 Pisa, Italy.

[17]NASA Marshall Space Flight Center, Huntsville, AL 35812, USA.

[18]Istituto Nazionale di Fisica Nucleare, Sezione di Torino, Via Pietro Giuria 1, 10125 Torino, Italy.

[19]Dipartimento di Fisica, Università degli Studi di Torino, Via Pietro Giuria 1, 10125 Torino, Italy.

[20]INAF Osservatorio Astrofisico di Arcetri, Largo Enrico Fermi 5, 50125 Firenze, Italy.

[21]Dipartimento di Fisica e Astronomia, Università degli Studi di Firenze, Via Sansone 1, 50019 Sesto Fiorentino (FI), Italy.

[22]Istituto Nazionale di Fisica Nucleare, Sezione di Firenze, Via Sansone 1, 50019 Sesto Fiorentino (FI), Italy.

[23]Science and Technology Institute, Universities Space Research Association, Huntsville, AL 35805, USA.

[24]Istituto Nazionale di Fisica Nucleare, Sezione di Roma "Tor Vergata", Via della Ricerca Scientifica 1, 00133 Roma, Italy.

[25]Department of Physics and Kavli Institute for Particle Astrophysics and Cosmology, Stanford University, Stanford, California 94305, USA.

[26]Institut für Astronomie und Astrophysik, Universität Tübingen, Sand 1, 72076 Tübingen, Germanyy.

[27]Astronomical Institute of the Czech Academy of Sciences, Boční II 1401/1, 14100 Praha 4, Czech Republic.

[28]California Institute of Technology, Pasadena, CA 91125, USA.

[29]Yamagata University,1-4-12 Kojirakawa-machi, Yamagata-shi 990-8560, Japan.

[30]Osaka University, 1-1 Yamadaoka, Suita, Osaka 565-0871, Japan.

[31]University of British Columbia, Vancouver, BC V6T 1Z4, Canada.

[32]School of Mathematics, Statistics and Physics, Newcastle University, Herschel Building, Newcastle upon Tyne, NE1 7RU, UK.

[33]Department of Physics, Faculty of Science and Engineering, Chuo University, 1-13-27 Kasuga, Bunkyo-ku, Tokyo 112-8551, Japan.

[34]International Center for Hadron Astrophysics, Chiba University, Chiba 263-8522, Japan.

[35]Institute for Astrophysical Research, Boston University, 725 Commonwealth Avenue, Boston, MA 02215, USA.

[36]Department of Astrophysics, St. Petersburg State University, Universitetsky pr. 28, Petrodvoretz, 198504 St. Petersburg, Russia.

[37]Department of Physics and Astronomy, University of Iowa, Iowa City, IA 52242, USA.

[38]Physics Department and McDonnell Center for the Space Sciences, Washington University in St. Louis, St. Louis, MO 63130, USA.

[39]Finnish Centre for Astronomy with ESO, 20014 University of Turku, Finland.

[40]MIT Kavli Institute for Astrophysics and Space Research, Massachusetts Institute of Technology, 77 Massachusetts Avenue, Cambridge, MA 02139, USA.

[41]Graduate School of Science, Division of Particle and Astrophysical Science, Nagoya University, Furo-cho, Chikusa-ku, Nagoya, Aichi 464-8602, Japan.

[42]Hiroshima Astrophysical Science Center, Hiroshima University, 1-3-1 Kagamiyama, Higashi-Hiroshima, Hiroshima 739-8526, Japan.

[43]University of Maryland, Baltimore County, Baltimore, MD 21250, USA.

[44]NASA Goddard Space Flight Center, Greenbelt, MD 20771, USA.

[45]Center for Research and Exploration in Space Science and Technology, NASA/GSFC, Greenbelt, MD 20771, USA.

[46]Department of Physics, The University of Hong Kong, Pokfulam, Hong Kong.

[47]Department of Astronomy and Astrophysics, Pennsylvania State University, University Park, PA 16802, USA.

[48]Department of Physics and Astronomy, 20014 University of Turku, Finland.

[49]INAF Osservatorio Astronomico di Brera, Via E. Bianchi 46, 23807 Merate (LC), Italy.

[50]Dipartimento di Fisica e Astronomia, Università degli Studi di Padova, Via Marzolo 8, 35131 Padova, Italy.

[51]Dipartimento di Fisica, Università degli Studi di Roma "Tor Vergata", Via della Ricerca Scientifica 1, 00133 Roma, Italy.

[52]Department of Astronomy, University of Maryland, College Park, Maryland 20742, USA.

[53]Mullard Space Science Laboratory, University College London, Holmbury St Mary, Dorking, Surrey RH5 6NT, UK.

[54]Anton Pannekoek Institute for Astronomy & GRAPPA, University of Amsterdam, Science Park 904, 1098 XH Amsterdam, The Netherlands.

[55]Guangxi Key Laboratory for Relativistic Astrophysics, School of Physical Science and Technology, Guangxi University, Nanning 530004, China.

Abstract

The center of the Milky Way Galaxy hosts a $\sim$4 million solar mass black hole (Sgr A*) that is currently very quiescent with a luminosity many orders of magnitude below those of active galactic nuclei [1]. Reflection of X-rays from Sgr A* by dense gas in the Galactic Center region offers a means to study its past flaring activity on times scales of hundreds and thousands of years [2]. The shape of the X-ray continuum and the strong fluorescent iron line observed from giant molecular clouds in the vicinity of Sgr A* are consistent with the reflection scenario [3-5]. If this interpretation is correct, the reflected continuum emission should be polarized [6]. Here we report observations of polarized X-ray emission in the direction of the Galactic center molecular clouds using the Imaging X-ray Polarimetry Explorer (IXPE). We measure a polarization degree of $31\% \pm 11\%$, and a polarization angle of $-48° \pm 11°$. The polarization angle is consistent with Sgr A* being the primary source of the emission, while the polarization degree implies that some 200 years ago the X-ray luminosity of Sgr A* was briefly comparable to a Seyfert galaxy.

Keywords: polarization, black holes, quasars, Galactic center

IXPE observed the molecular complex Sgr A, the X-ray brightest group of reflection clouds near Sgr A* [7], for an exposure of 0.93 megaseconds after filtering in February and March 2022. Contemporaneous Chandra X-ray Observatory observations with high angular resolution were acquired to identify regions where the reflected emission is strong and to extract spectra from these regions. Fig. 1 shows the X-ray surface brightness maps in the 4–8 keV band obtained. We excluded X-rays below 4 keV since they arise from unpolarized

plasma emission [8-10], see Fig. 6. See the Methods section for details on the observations and data reduction.

Based on the Chandra image only, we selected a circular extraction region with a radius $4.5'$ centered on the Sgr A complex that contains numerous hot spots of reflected emission (i.e. scattering clouds). This region was selected to collect as many 'reflected' photons as possible while avoiding the edges of the IXPE detectors. The region includes most areas of elevated reflected emission. The region excludes areas affected by very bright sources that enter the IXPE field-of-view as a result of the pointing dithering pattern and a bright $1'$ region associated with the non-thermal object G0.13-0.11 [11] to avoid possible contamination of the polarised signal.

Fig. 2 shows good agreement between the spectra extracted from IXPE, Chandra, and archival XMM-Newton data for the selected region. A bump, associated with iron lines at 6.4 and 6.7 keV, is clearly seen, even with IXPE's lower spectral resolution. The model based on XMM-Newton and Chandra data well describes the IXPE spectrum, given the current level of cross-calibration uncertainties between the instruments.

The spectral model is built from several components: thermal and reflected emission, fluorescent lines, and scattered continuum (see Methods). All of them, except for the component representing the reflected emission from the molecular cloud, are assumed to be constant in time, i.e. the same for all three datasets. The reflected emission is a combination of Compton scattered and photo-absorbed continuum with fluorescent emission lines calculated self-consistently from the reflection spectrum [12]. Only the continuum part of the reflected spectrum is expected to be polarized [9,10,13]. Hence, the X-ray polarization (described by the Stokes parameters Q and U measured by IXPE) is related to the reflection continuum $I_{\mathrm{refl,c}}$, and not to the total observed intensity I [14-15]. Polarization degree is independent of photon energy in the single-scattering scenario, so the spectral shape of Q and U follow that of $I_{\mathrm{refl,c}}$.

Fig. 3 shows the observed Q and U spectra. The Q values are close to zero, while U is mostly negative, suggesting a polarization angle close to $-45°$. The best-fitting reflection model is shown with solid lines. Here, we have explicitly assumed that all emission from the selected region has the same polarisation degree and angle, which is valid if the illuminated group of clouds is compact in 3D. With these simplifying assumptions, our model has only two free parameters derived from the IXPE data: degree of polarization $P = 31 \pm 11\%$ and polarisation angle $\phi = -48° \pm 11°$ (uncertainties are 68% confidence level, see Fig. 4; ϕ is anti-clockwise from North in the equatorial coordinate system per IAU convention). As explained in Methods, the absolute normalization of the reflected component has ~30% uncertainty. Therefore, the constraints on the polarization degree are a multiplicative combination of statistical and systematic uncertainties: $P = (0.31 \pm 0.11)_{\mathrm{stat}} \times (1.0 \pm 0.3)_{\mathrm{sys}}$. Even with this extra uncertainty, it is clear that the observed polarization degree is significantly smaller than 100%. The systematic uncertainty does not affect the significance of the polarized signal detection, which corresponds to ~ 2.8 standard deviations.

The measured polarization angle ϕ is consistent with the hypothesis that Sgr A* is the primary source (see Fig. 4). For a cloud located at the center of our extraction region, the line orthogonal to the direction towards Sgr A* corresponds to $\phi = -42°$. This is within the uncertainties of our measurement ($\phi = -48° \pm 11°$), so fixing the measured polarization angle to $-42°$ does not affect the errors on the degree of polarisation.

The degree of polarisation P of the reflected continuum is directly related to the scattering angle θ in the single scattering approximation, $P = (1 - \mu^2)/(1 + \mu^2)$, where $\mu = \cos\theta$. Any value of P produces two solutions, θ and $\pi - \theta$. For $P = 31 \pm 11\%$, the solutions are 43^{+7}_{-8} and 137^{-7}_{+8} degrees. A similar level of uncertainty is caused by the $\sim 30\%$ systematic error in the value of P. These angles fix the scattering geometry, the smaller value corresponds to clouds between us and the primary source and the larger to clouds beyond the source (see Methods).

For a given scattering angle θ, one can also calculate the age of the flare t_{flare}, i.e. the time delay associated with the propagation of X-rays from the primary source to the cloud and then to the observer. Adopting a projected distance between Sgr A* and the scattering clouds of 25 pc, i.e. the distance between the SMBH and the centre of our extraction zone in the sky plane, the two solutions for θ translate into two t_{flare} values: 33^{+6}_{-7} and 205^{-30}_{+50} years, respectively. Again, the systematic uncertainties are comparable to the quoted statistical errors (see Methods). From the point of view of polarization properties, both solutions are equivalent. However, the 'older' flare is far more plausible. First of all, for the cloud located well behind the primary source, the propagation speed of the light front of the flare approaches $c/2$ [16], where c is the speed of light, while for the cloud in front of the primary source, this speed is always greater than c. Thus, for a short flare, a cloud located behind Sgr A* will remain bright longer than the same cloud in front of it, and, therefore, on average, the chances to spot it in a bright phase are higher. Secondly, the 'younger' flare from Sgr A* would have been observed directly. Indeed, the Advanced Satellite for Cosmology and Astrophysics (ASCA) was active 30 years ago; the GMCs were bright at the time [5,17], while Sgr A* was not. The Sgr B2 cloud, which in the sky plane is much further away from Sgr A* than the area covered by IXPE, was bright too. This fact strongly suggests that the flare is significantly older than 30 years, or that there were multiple flares. Here, the former scenario is adopted and is consistent with the range of values found in the literature ($100 - 500$ years, depending on the methods and Galactic center regions probed [18-21]).

Our work presents the missing piece of evidence that X-rays from the giant molecular clouds are due to reflection of an intense, yet short-lived flare produced at or nearby Sgr A*. These results can further constrain the past activity of the Galactic center. The observational data provide a flare fluence (product of the luminosity L_X and duration Δt of the flare) of a few 10^{47} erg [12,22]. Based on previous studies of the X-ray variability of small molecular clouds in reflected emission, the duration of the flare is $\Delta t < 1.6\,\mathrm{yr}$ [22]. Existing

observational data [12,22], including those of IXPE (see Methods), suggest the broad-band (1–100 keV) flare luminosity was in the range from a few 10^{39} to $\sim 10^{44}$ erg s^{-1}, i.e. comparable to the X-ray luminosity of Seyfert galaxies [23,24]. The lower limit comes from the brightest levels of the surface brightness observed over years (see Methods), while the upper limit corresponds to the Eddington luminosity of Sgr A*, which could be exceeded in some scenarios. Given the fluence constraint, the lowest luminosity requires a 1–2 year-long flare, while the highest luminosity needs only an hour-long outburst.

Potential origins of flares with the needed fluence [25] include accretion induced collapse of white dwarfs, sub-luminous gamma-ray bursts, tidal disruption events, or transient accretion onto SMBHs not related to tidal disruption. Classes of transients that can be excluded because their luminosities fall short by a factor of 10–100 include giant flares from soft gamma-ray repeaters (magnetars), type II supernova breakouts, and major outbursts of ultra-luminous X-ray sources. The second line of reasoning could come from the comparison of the expected event rates, bearing in mind that the fluence was calculated for the adopted distance between the clouds and Sgr A*, and, therefore, the assumption that the source is further away would boost the required fluence. These considerations favor Sgr A* as the prime candidate, especially considering the consistency of its position with the measured polarization degree, although other scenarios are not completely eliminated.

Detection of the faint and diffuse X-ray emission due to reflection from molecular clouds in the Galactic Center region remains a challenging exercise. Current IXPE data demonstrate this goal is within the reach of IXPE, paving a way for future, even longer observations that will enable more detailed analysis, including spatially resolved polarisation, to verify the single flare scenario, and the determination of the intrinsic polarization of the flares to probe the origin of the radiation and constraints on the multiple-flare scenarios.

Author contributions. F. Marin led the IXPE observation, contributed to the analysis and led the writing of the paper. E. Churazov, I. Khabibullin, R. Ferrazzoli, L. Di Gesu, T. Barnouin, A. Di Marco, R. Middei, E. Costa, P. Soffitta, F. Muleri, R. Sunyaev and P. Kaaret contributed to the IXPE analysis, discussion and writing of the paper. A. Vikhlinin, W. Forman and R. Kraft provided and reduced the Chandra data used in this paper. S. Bianchi, D. Immacolata, P.-O. Petrucci and T. Enoto contributed with discussion and parts of the paper. The remaining authors are part of the IXPE team whose significant contribution made the satellite and the Galactic center observation possible.

Author information. The main author can be contacted using his official e-mail address : frederic.marin@astro.unistra.fr

Competing interest. Authors declare that they have no competing interests.

Data availability. The IXPE data that support the findings of this study are freely available in the HEASARC IXPE Data Archive (https://heasarc.gsfc.nasa.gov/docs/ixpe/archive/). The XMM-Newton data can be found on the same website, while the Chandra data will be public after one year from the observation date.

Code availability. The analysis and simulation software *ixpeobssim* developed by IXPE collaboration and its documentation is available publicly through the web-page https://ixpeobssim.readthedocs.io/en/latest/?badge=latest.494. XSPEC is distributed and maintained under the aegis of the HEASARC and can be downloaded as part of HEAsoft from http://heasarc.gsfc.nasa.gov/docs/software/lheasoft/download.html.

(a)   (b)
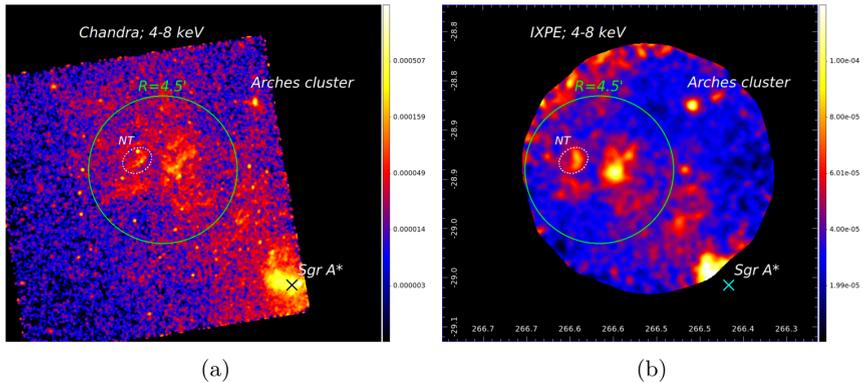
Fig. 1: **Quasi-simultaneous Chandra (a) and IXPE (b) 4–8 keV X-ray surface brightness maps of the Galactic center region to the North-East from Sgr A∗.** The maps are in equatorial coordinates, North is up. The IXPE image is in units of counts s^{-1} arcmin^{-2} cm^{-2} colour-coded on a linear scale (see the colorbar on the right). For IXPE, the edges of the image, where the exposure (including vignetting effects) drops below 15% of the maximal value, have been truncated [26]. For Chandra, the image units are the same but a logarithmic scale is used to show both diffuse and compact sources. The positions of the supermassive black hole Sgr A∗ and the Arches star cluster are labeled. The area where reflection emission is strong in the Chandra data is shown using a green 4.5′ radius circle. This circle was used to extract I, Q, and U spectra from the IXPE data. The same region was used for Chandra and XMM-Newton spectral analysis. The white dashed ellipse shows the location of a bright non-thermal (NT) source G0.13-0.11 [11] that was excluded for the spectra extraction.

Table 1: Observations used in this work for background extraction.

Mission	Obs.ID	Start date (YYYY-MM-DD)	Effective exposure (kiloseconds)	Notes
IXPE	1003701	2022-05-04	96.7	Mrk421
IXPE	1003801	2022-06-04	96.0	Mrk421
IXPE	1004501	2022-03-08	100.4	Mrk501
IXPE	1004701	2022-07-09	97.8	Mrk501
IXPE	1006301	2022-05-06	390.9	BL Lac
IXPE	1006301	2022-05-06	116.9	BL Lac
IXPE	1003501	2022-07-12	771.8	Circinus
IXPE	1005701	2022-06-12	264.2	3C279
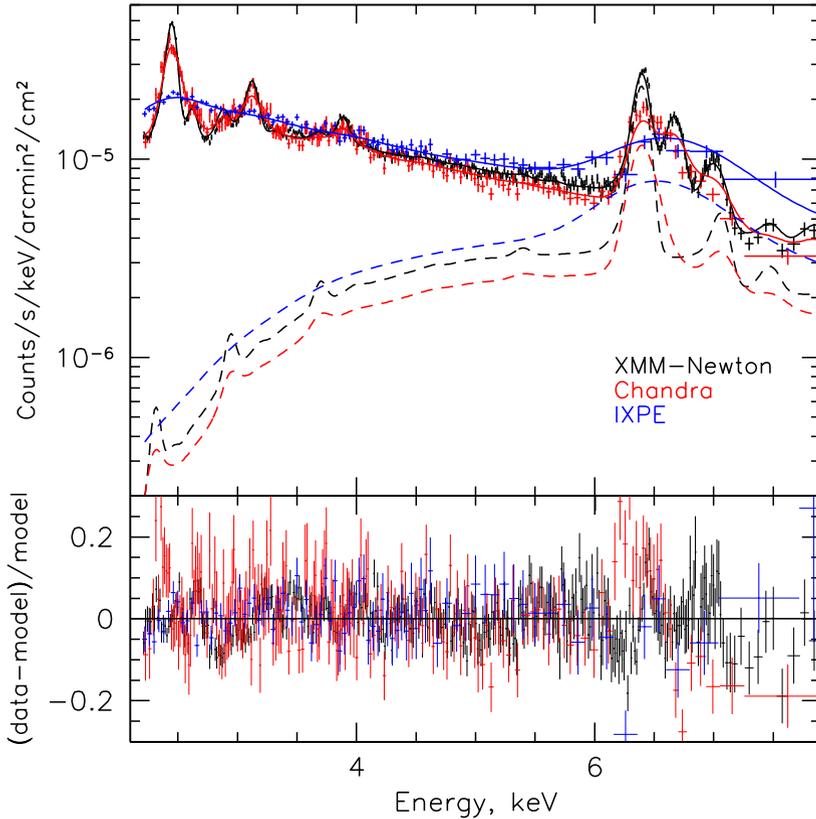
Fig. 2: **Spectra of the X-ray emission extracted from the circular region shown in Fig. 1 obtained in Chandra (red), IXPE (blue) and archival XMM-Newton (black) observations, after division by energy-dependent effective area of each telescope.** Errorbars correspond to 1σ (68% confidence intervals). The solid lines correspond to the best-fitting models (three thermal components and the reflection emission, see Methods) convolved with the telescopes' spectral responses, resulting in strong smearing of the emission lines in the IXPE data. Parameters of the thermal components were fixed among all three datasets, and only the normalization of the reflection component was allowed to vary between them. The dashed lines show the best-fitting contribution of the reflected emission to the total spectrum for each of the three instruments. The difference in the normalization of the reflected emission ($\sim 30\%$) could be caused by the time variability and the different energy-dependent efficiencies of the three telescopes. As demonstrated by the residuals shown in the second panel, the model provides a reasonable approximation of the data (at the level of $\sim 20\%$) even although with high statistics of the XMM-Newton and Chandra data a few wiggles near the bright emission lines are visible, which are plausibly caused by slight gain variations among the data sets.
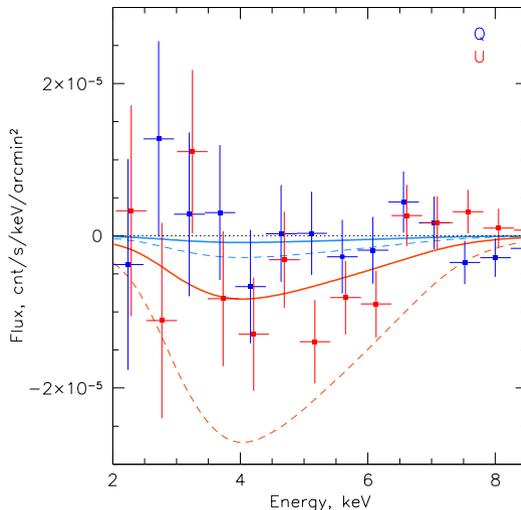
Fig. 3: **Stokes parameters Q (blue) and U (red) spectra extracted from the circular region shown in Fig. 2.** Errorbars correspond to 1σ (68% confidence intervals). For clarity, both the Q and U data points are slightly shifted in energy. The solid blue and red lines represent the best fitting reflection model (the Compton-scattered continuum component only) to the Q and U spectra with a degree of polarization 31% and the polarization angle $-48°$. The model has been convolved with the IXPE spectral response. The thinner dashed lines are representative of the maximum Q and U that one could expect for $90°$ scattering that would lead to a 100% polarized reflected continuum.

Table 2: The three more intense sources and their re-scaled flux in the extraction region we used in our paper (see Fig. 1). Fluxes are in erg s^{-1} cm^{-2}.

Source	Flux	Angular sep. (°)	Suppression factor	Re-scaled flux
2CXO J174621.1-284343	5.033E-11	0.22	245	1.4E-13
2CXO J174451.6-292042	3.949E-11	0.52	752	3.4E-14
2CXO J174445.4-295045	3.387E-11	0.964	1120	2.0E-14
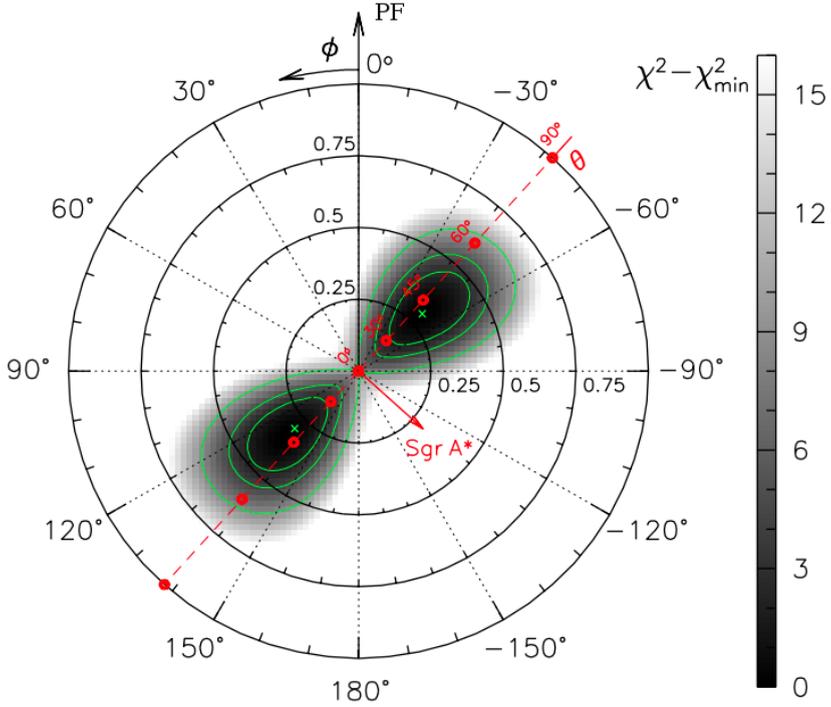
Fig. 4: **Map of the $\chi^2 - \chi^2_{\min}$ statistic for the fit of the Stokes parameters Q and U spectra.**,We used the reflection continuum model in polar coordinates with radius equal to the polarization fraction (PF) and the azimuthal angle showing the position angle of the electric field vector (ϕ). The minimal value of the statistic $\chi^2_{\min}$ corresponds to the best fitting values $\phi = -48°$ and $P = 31\%$ (marked as green crosses), and the contours show 68, 90 and 99% confidence levels. The hypothesis that Sgr A* is the primary source of illuminating X-ray flux, implies the polarization angle $\phi = -42°$ for the center of the region used for extraction of the Q and U spectra, as marked with the red dashed line. The circles on this line depict expected polarization degrees for the scattering angle changing from 0(180) to 30(150), 45(135), 60(120), and 90 degrees.

(a)

(b)

(c)
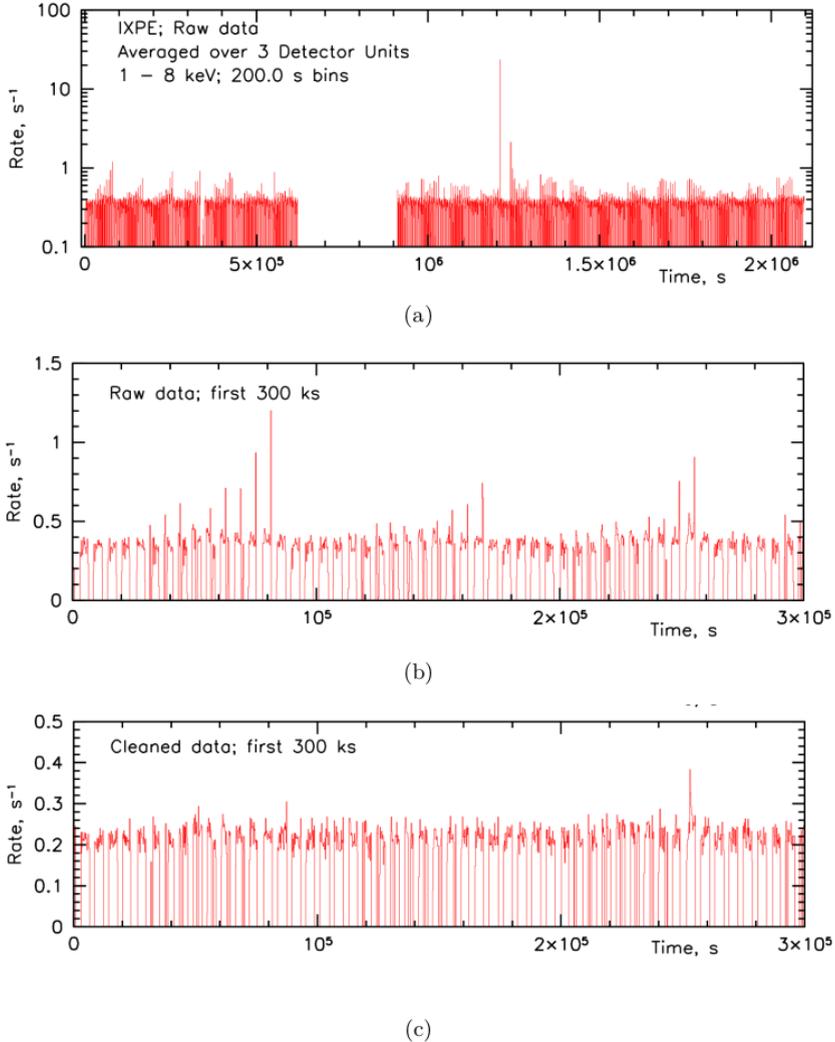
Fig. 5: **Illustration of the data cleaning prior to the imaging and spectral analysis.** Panel (a) shows the count rate in the 2–8 keV band (sum of three DUs, 200 seconds time bins) in the original data set that spans 2 million seconds. The two most intense spikes are associated with a geomagnetic storm. To illustrate less prominent variations, panel (b) shows a 300 kiloseconds-long portion of the same light curve that feature a number of smaller amplitude quasi-regular spikes (notice that the vertical scale has changed) that are mostly due to the South Atlantic Anomaly. The gaps in the light curves correspond to moments when the Galactic center was obscured by the Earth. Finally, panel (c) shows the count rate for the data cleaned from spikes and individual events that most plausibly are due to detector background rather than X-ray photons. The overall count rate in the cleaned data is almost a factor of two lower than in the original data.
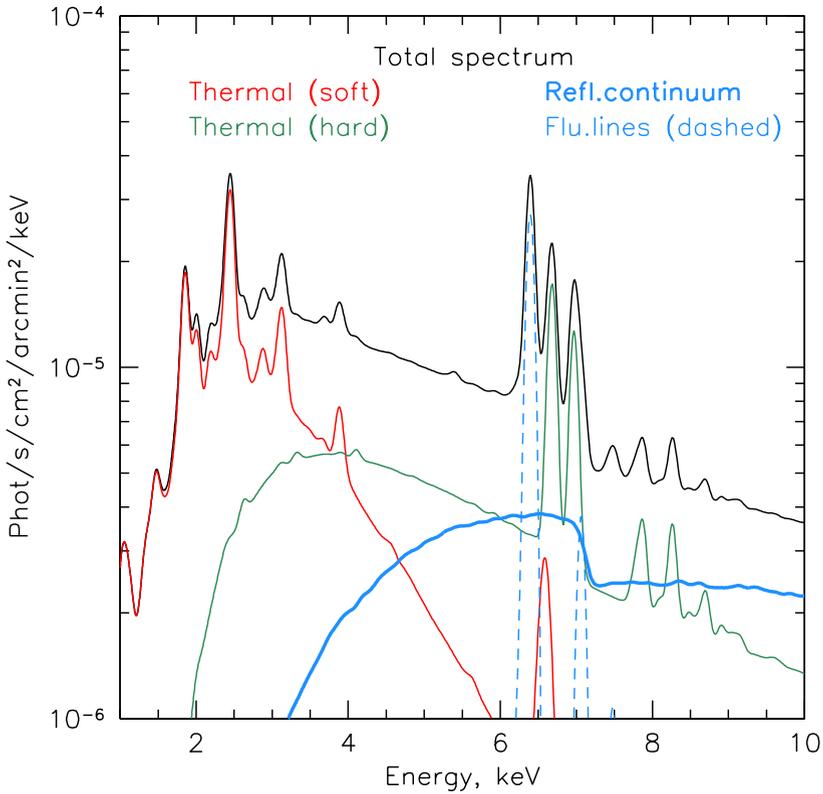
Fig. 6: **An illustration of the spectral model used to approximate X-ray spectra extracted from the reference region.** For clarity, only two "thermal" components are shown in the plot. The red and the green curves are those thermal components, detailed in [45,46]. The hotter (green) of the models, having prominent lines at 6.7 and 6.97 keV, contributes significantly to the 4–8 keV band. The blue curves show the two components of the reflected emission. Namely, the dashed blue curves show the fluorescent lines of iron (Kα line at 6.4 keV and Kβ line at 7.06 keV), while the thick blue line shows the scattered continuum. Only the latter component is polarized and used to fit the Q and U spectra measured by IXPE. The black line shows the sum of all components. In order to show more clearly the components of the physical model in units of photons $\mathrm{s}^{-1}\,\mathrm{cm}^{-2}\,\mathrm{arcmin}^{-2}\,\mathrm{keV}^{-1}$ the spectra were convolved with a Gaussian, which is narrower than the energy resolution of the IXPE, Chandra, and XMM-Newton detectors.

References

[1] Reinhard Genzel, Frank Eisenhauer, and Stefan Gillessen. The Galactic Center massive black hole and nuclear star cluster. Reviews of Modern Physics, 82(4):3121–3195, October 2010.

[2] L. A. Vainshtein and R. A. Syunyaev. The K-Alpha Lines in the Background X-Ray Spectrum and the Interstellar Gas in Galaxies. Soviet Astronomy Letters, 6:353–356, June 1980.

[3] R. A. Sunyaev, M. Markevitch, and M. Pavlinsky. The Center of the Galaxy in the Recent Past: A View from GRANAT. Astrophysical Journal, 407:606, April 1993.

[4] M. Markevitch, R. A. Sunyaev, and M. Pavlinsky. Two sources of diffuse X-ray emission from the Galactic Centre. Nature, 364(6432):40–42, July 1993.

[5] Katsuji Koyama and et al. ASCA View of Our Galactic Center: Remains of Past Activities in X-Rays? Publications of the Astronomical Society of Japan, 48:249–255, April 1996.

[6] E. Churazov, R. Sunyaev, and S. Sazonov. Polarization of X-ray emission from the Sgr B2 cloud. Monthly Notices of the Royal Astronomical Society, 330(4):817–820, March 2002.

[7] Ildar Khabibullin, Eugene Churazov, and Rashid Sunyaev. SRG/eROSITA view of X-ray reflection in the Central Molecular Zone: a snapshot in September-October 2019. Monthly Notices of the Royal Astronomical Society, 509(4):6068–6076, February 2022

[8] M. Revnivtsev and et al. Discrete sources as the origin of the Galactic X-ray ridge emission. Nature, 458(7242):1142–1144, April 2009.

[9] L. Di Gesu and et al. Prospects for IXPE and eXTP polarimetric archaeology of the reflection nebulae in the Galactic center. Astronomy and Astrophysics, 643:A52, November 2020.

[10] R. Ferrazzoli and et al. Prospects for a polarimetric mapping of the Sgr A molecular cloud complex with IXPE. Astronomy and Astrophysics, 655:A108, November 2021.

[11] Q. Daniel Wang, Fangjun Lu, and Cornelia C. Lang. X-Ray Thread G0.13-0.11: A Pulsar Wind Nebula? Astrophysical Journal, 581(2):1148–1153, December 2002.

[12] E. Churazov, I. Khabibullin, G. Ponti, and R. Sunyaev. Polarization and

long-term variability of Sgr A* X-ray echo. Monthly Notices of the Royal Astronomical Society, 468(1):165–179, June 2017.

[13] F. Marin, F. Muleri, P. Soffitta, V. Karas, and D. Kunneriath. Reflection nebulae in the Galactic center: soft X-ray imaging polarimetry. Astronomy and Astrophysics, 576:A19, April 2015.

[14] F. Kislat, B. Clark, M. Beilicke, and H. Krawczynski. Analyzing the data from X-ray polarimeters with Stokes parameters. Astroparticle Physics, 68:45–51, August 2015.

[15] Ildar Khabibullin, Eugene Churazov, and Rashid Sunyaev. Impact of intrinsic polarization of Sgr A* historical flares on (polarization) properties of their X-ray echoes. Monthly Notices of the Royal Astronomical Society, 498(3):4379–4385, September 2020.

[16] R. Sunyaev and E. Churazov. Equivalent width, shape and proper motion of the iron fluorescent line emission from molecular clouds as an indicator of the illuminating source X-ray flux history. Monthly Notices of the Royal Astronomical Society, 297(4):1279–1291, July 1998.

[17] Shigeo Yamauchi, Yoshitomo Maeda, and Katsuji Koyama. ASCA observation of the Galactic Center. Advances in Space Research, 19(1):63–70, May 1997.

[18] Syukyo G. Ryu, Katsuji Koyama, Masayoshi Nobukawa, Ryosuke Fukuoka, and Takeshi Go Tsuru. An X-Ray Face-On View of the Sagittarius B Molecular Clouds Observed with Suzaku. Publications of the Astronomical Society of Japan, 61:751, August 2009.

[19] Syukyo Gando Ryu and et al. X-Ray Echo from the Sagittarius C Complex and 500-year Activity History of Sagittarius A*. Publications of the Astronomical Society of Japan, 65:33, April 2013.

[20] R. Terrier and et al. Fading Hard X-ray Emission from the Galactic Center Molecular Cloud Sgr B2. Astrophysical Journal, 719(1):143–150, August 2010.

[21] D. Chuard and et al. Glimpses of the past activity of Sgr A* inferred from X-ray echoes in Sgr C. Astronomy and Astrophysics, 610:A34, February 2018.

[22] E. Churazov, I. Khabibullin, R. Sunyaev, and G. Ponti. Can Sgr A* flares reveal the molecular gas density PDF? Monthly Notices of the Royal Astronomical Society, 471(3):3293–3304, November 2017.

[23] A. Ptak. Low-luminosity AGN and normal galaxies. In Nicholas E. White,

Giuseppe Malaguti, and Giorgio G. C. Palumbo, editors, X-ray Astronomy: Stellar Endpoints, AGN, and the Diffuse X-ray Background, volume 599 of American Institute of Physics Conference Series, pages 326–335, December 2001.

[24] Eve L. Halderson, Edward C. Moran, Alexei V. Filippenko, and Luis C. Ho. The Soft X-Ray Properties of Nearby Low-Luminosity Active Galactic Nuclei and their Contribution to the Cosmic X-Ray Background. Astronomical Journal, 122(2):637–652, August 2001.

[25] Alicia Soderberg and et al. The Dynamic X-ray Sky of the Local Universe. In astro2010: The Astronomy and Astrophysics Decadal Survey, volume 2010, page 278, January 2009.

[26] Martin C. Weisskopf and et al. The Imaging X-Ray Polarimetry Explorer (IXPE): Pre-Launch. Journal of Astronomical Telescopes, Instruments, and Systems, 8(2):026002, April 2022.

Methods

IXPE and Chandra observation

The molecular complex Sgr A is currently the brightest collection of reflection clouds in X-ray emission around Sgr A* [27]. This region, centered on Right Ascension $266.51°$ and Declination $-28.89°$ in equatorial coordinates, was pointed by IXPE [28] with a total integration time of 0.93 megaseconds (324 kiloseconds from February 27 to March 6, 2022, and 639 kiloseconds from March 10 to March 24, 2022), after filtering for episodes of enhanced instrumental background.

In addition to the X-ray polarimetric data, a few quasi-simultaneous observations with the Chandra X-ray observatory were acquired from February 26 to March 11, 2022 using the ACIS-I detector (OBSIDs 24373, 24820, and 26353), which cover the 0.3–10.0 keV band with a spectral resolution of $\Delta E \sim 0.3$ keV near $E = 6$ keV and arcsecond angular resolution. The Chandra high angular resolution data were essential to identify regions where the reflected emission is strong and to extract spectra from these regions.

IXPE data reduction

The IXPE observatory, as described in detail in [28], includes three identical X-ray telescopes, each comprising an X-ray mirror module assembly (provided by NASA) and a polarization-sensitive Gas Pixel Detector (GPD, provided by the Italian side of the collaboration), to offer spatially resolved X-ray polarimetry in the 2–8 keV energy band. At the Science Operations Center (SOC, at the NASA Marshall Space Flight Center), a software pipeline developed jointly by ASI and NASA processes the relevant science, engineering and ancillary data, estimates the photoelectron emission direction (and hence the polarization), position, and energy of each event after applying corrections for charging effects of the Gas Electron Multiplier (GEM), detector temperature, and gain non-uniformity. The use of the IXPE on-board calibration sources [29] allows correction for time-and-spatially-dependant gain variations of the detectors. The in-flight calibration measurements provide the best knowledge of the gain of the detectors at the time of the observation, and hence the correct energy of each photon, needed to correct the Stokes parameters for the presence of spurious polarization, and to use the correct value of the modulation factor (the modulation amplitude for a 100% linearly polarized radiation [28]). The removal of spurious polarization is achieved using the algorithm of [30].

The output of this pipeline processing is an event file in FITS format for each of the three IXPE detector units that, in addition to the typical information related to spatially resolved X-ray astronomy, contains the event-by-event Stokes parameters [see 31] from which the polarization of the radiation can be derived. The data products are archived at the High-Energy Astrophysics

Science Archive Research Center (HEASARC, at the NASA Goddard Space Flight Center), for use by the international astrophysics community. These level-2 event files were cleaned from additional environmental and background contamination [32].

In the case of the observation of the Galactic center, the observation window corresponded to a period of increased solar activity which led to an increase of atmospheric noise (particle background). In addition, such activity tends to extend the South Atlantic Anomaly (SAA), above which the detectors are usually turned off to prevent observation in a highly particle polluted environment. However, as can be seen on Fig. 5 (panel a), several spikes were recorded in the light-curve right before the spacecraft entry in the SAA. Using the v26.0.0 ixpeobssim tool (available here : https://ixpeobssim.readthedocs.io/en/latest/) [33], we removed the count spikes associated with Earth occultation periods and above the extended SAA. Some spurious events attributed to geomagnetic storm events were also flagged and excised. New good time intervales (GTIs) were then computed using these prolonged epochs and allowed event filtering based on the presence of unaccounted atmospheric noise. After GTI correction (Fig. 5, panel c), the livetime (or Total Good Time) is 0.93 Ms, which represent 96.7% of the livetime before filtering.

IXPE systematic effects

All systematic errors are well below the polarization degree and angle observed from the 4.5′ extraction circle we used in this paper. Below, we give a brief statement on each of the sources of potential systematic effects and refer to the pre-launch papers for a deeper analysis [32,34]:

- **Instrumental and extra-galactic backgrounds.** From the stacking of almost 2 million seconds worth of background-rejected data from annular background regions around extra-galactic point sources (see Tab. 1, we also excluded sources bright enough to pollute the background extraction region with their signal because of the wing of the point-spread-function), the background is unpolarized down to a minimum detectable polarization of 3.7% at 99% confidence level. This is well below the measured polarization from the Sgr A region presented in this work.
- **Spurious polarization.** The spurious polarization we managed to calibrate in a 4.5' radius amounts for 0.05%. The statistical error on the derived polarization measurement is 11% (or about 4% modulation). As a consequence, the residual systematic polarization has no effect on the results presented in this paper.
- **Stray light.** The IXPE requirement on the level of stray light is that its suppression should be larger than a factor of 200 (verified at 2.3 keV). We re-scaled the suppression coefficient of the three more intense sources outside the 4.5' radius circle used in this paper as found in the Chandra catalogue (see Tab. 2). The resulting stray-light counting rate (0.5–7 keV) from these

sources outside the field of view are 10 μCrab at most (Crab 0.5–7 keV = 2.8×10^{-8} erg s^{-1} cm^{-2}). Assuming that these sources are 10% polarized, the effect on the observed counting rate is at most 0.1%, i.e. negligible.

- **Solar Effects.** Due to the thick shielding of the detectors, only in case of a very bright X Class solar flare a few photons have been detected (cross-matched by monitoring satellites). Data in coincidence of solar flares are simply removed. In addition, spikes due to passages over the SAA were also removed, as stated previously, and thus do not contribute to systematic effects.
- **Effects related to Earth atmosphere.** The Earth atmosphere, during most of observations, crosses the field of view of IXPE at each orbit. The data are excluded from the analysis. In any case, the atmosphere is dark in the range of IXPE and becomes bright above 10 keV. So we can state that the albedo of Earth is never directly observed by IXPE telescopes. Indirectly, namely through scattering, it contributes to the instrumental background. In fact the satellite orbits the Earth with an angular velocity of 360° in 90 minutes, which is 4° per minute. This means that the source is seen on the limb of the Earth only within 13', which is 3 seconds each orbit.

Chandra data reduction

The Chandra data reduction follows a standard procedure based on the latest versions of the data reduction software (CIAO v. 4.14) and calibration (CALDB v. 4.9.8). Our particular approach and analysis steps are described in detail in [35]. Briefly, they include identification and removal of high background periods, correction of photon energies for the time and detector temperature dependence of the charge transfer inefficiency and gain, and creation of matching background datasets using blank sky observations with exposure times similar to the Galactic Center pointings.

The Chandra observing program included multiple pointings with individual exposures 10–30 kiloseconds. Due to the spacecraft orientation relative to the Sun, many observations were done with the ACIS focal plane temperature significantly higher than a nominal value of -120 C, resulting in potential problems with the detector gain and response calibration. To minimize the impact of this issue, we have used three Chandra pointings (OBSIDs 24373, 24820, and 26353) with the lowest focal plane temperatures ($T < -116.5$ C) and that were done quasi-simultaneously with the IXPE observations (February 26 through March 11), with a total exposure of 52 kiloseconds.

For the analysis presented here, we use the combined flat-fielded and background-subtracted Chandra image in the 4–8 keV band, and spectra extracted in 4.5$'$ circular region discussed above. Following the standard approach for analysing Chandra spectra of extended sources, we have generated the spectral response files that combine the position-dependent ACIS calibration with the weights proportional to the observed brightness in the 4–8 keV band. The extracted spectral data and response files are fit to a set of models as described below.

To assess the impact of the calibration uncertainties associated with the elevated focal plane temperature, we repeated all analyses using the OBSIDs with higher temperatures than the three pointings used in this work. These experiments have shown that after the standard temperature-dependent corrections implemented in CIAO, the parameters of interest for this work (e.g., the 4–8 keV flux of the reflected component) are almost unchanged. Therefore, we conclude that the impact of elevated focal plane temperatures on our analysis is negligible.

Archival observations with XMM-Newton

In order to better constrain spectral de-composition of the X-ray emission from the region of interest, we have used all archival observations with XMM-Newton observatory accumulated between 2002 and 2012. These data have already been used for studies of the reflection component [36]. The XMM-Newton data were prepared, reduced and processed in exactly the same manner. As the final step, the spectrum was extracted from the same region as used by IXPE. Thanks to large effective area above 4 keV and long total exposure time supplemented with superior spectral resolution around 6 keV, the XMM-Newton data allow us to better separate thermal and reflected components. Since only the contribution of the reflected component is expected to vary over time, one can combine the archival data with the quasi-simultaneous Chandra and IXPE observations by allowing only parameters of the reflected component model to vary while linking parameters of all other components when fitting the spectra of the total emission observed by all three observatories.

Combined analysis of IXPE, Chandra, and XMM-Newton data

As the first step of the joint IXPE, Chandra and XMM-Newton analysis, the background-subtracted spectra extracted from the circular region shown in Fig. 1 have been fitted with the same multi-component model.

This model includes a reflection component and three "thermal" components (an illustrative example of the spectral model is shown in Fig. 6). The latter components can be approximated as emission of optically thin thermal plasma, even though they might now be indeed associated with diffuse X-ray emitting gas. Indeed, in the 4–8 keV energy band, the most important is the thermal component with temperature $kT \sim 6$ keV, which is plausibly due to cumulative emission of large number of point sources, mostly accreting white dwarfs and stars with active coronae [37]. The APEC model (see http://www.atomdb.org/) was used for the optically thin thermal components. The reflection component describes the spectrum emerging from a spherical cloud of molecular gas, illuminated by a beam of X-rays, having a power-law spectrum. For this purpose, a publicly available CREFL16 model [36] was used,

and more specifically a version of it where reflected continuum and fluorescent lines are treated separately but with tied parameters. CREFL16 is a model describing the spectrum of a uniform gas cloud illuminated by a parallel beam of X-rays. The model covers the energy range from 0.3 to 100 keV. It has 5 parameters: the Thomson optical depth of the cloud, the photon index of the incident spectrum, the abundance of heavy elements, the cosine of the angle between the line of sight and the illuminating angle, and the normalization. The softer thermal components are needed to properly describe the line-rich spectrum at energies below 3-4 keV (see Fig. 2). Similarly to the hotter component discussed above, the exact nature of these components is still a matter of debate [38].

A combination of all components provides a reasonably good approximation of the IXPE, Chandra, and archival XMM-Newton spectra extracted from the reference region. XSPEC version 12.10.1f was used for fitting the spectra of Chandra, XMM-Newton, and IXPE. For IXPE, XSPEC was also used to fit the Q and U spectra too. We note in passing that IXPE and Chandra observations are quasi-simultaneous, while the XMM-Newton data were averaged over several observations spread over many years (from 2002 to 2012). For that reason, the normalization of the reflected component in the XMM-Newton model was decoupled from the IXPE and Chandra models. All other components/parameters were tied across all three instruments. A standard χ^2 minimization has been used to fit all spectra (polarized and total). This approach is suitable for the IXPE, XMM-Newton, and Chandra data sets used here. The best-fitting spectral model (Fig. 2) to the combined data set of three instruments has a $\chi^2 = 1400$ for 922 degrees of freedom. the residuals shown in the second panel of Fig.2 is of the order of $\sim 20\%$, providing a reasonable approximation of the data. The excess of the χ^2 above expectations ($\chi^2 = 922 \pm 43$ at the 68% confidence) for the genuine model is not surprising given the simplicity of the model used here and, also, modest cross-calibration issues among all three telescopes.

The outcome of the spectral fitting model was in particular the normalization of the reflected component (expressed in units of surface brightness) and the parameters of the best-fitting CREFL16 model, which do not affect significantly the results of the IXPE data analysis. Critically assessing the spectral decomposition shown in Fig. 2, we concluded that a systematic uncertainty of order 30% is associated with the derived normalization of the reflected component. Since only the scattered continuum of the reflected component is polarized (ignoring second order effects caused by multiple scatterings, [39,40]), it was singled out and used to fit Q and U spectra measured by IXPE as shown in Fig. 3. For that fit, the scattered continuum component was multiplied by the effective area appropriate for the extraction region (taking into account vignetting) and the modulation factor. For Q and U spectra, the dependence on the polarization angle ϕ was accounted for by introducing multiplicative factors $\cos 2\phi$ and $\sin 2\phi$ in front of the scattered continuum component, for

Q and U, respectively. Namely, for the Thomson scattering,

$$Q(E) = P \cos 2\phi \times S(E)$$
$$U(E) = P \sin 2\phi \times S(E),$$

where $S(E)$ is the spectrum of the scattered continuum as derived from the spectral analysis and P is the degree of polarization. This model is valid in the single scattering approximation, and for a compact scattering cloud. From these expressions, it is clear that P is degenerate with the normalization of $S(E)$, but it does not affect the detection significance of non-zero polarization. This allows one to use a multiplicative notation when quoting the polarization degree as $P = (31 \pm 11)\% \times (1 \pm 0.3)$, where the second term arises from the uncertainties in the reflected continuum normalization.

The best-fitting model to the Q and U spectra (Fig. 3) has a $\chi^2 = 254.4$ for 248 unbinned channels and two free parameters - the normalization of the polarized component and the polarization angle. In the figure, the channels were grouped (12 channels per bin) for display purposes.

Sgr A* flare parameters

More than a century ago, Kapteyn [41] realized that for a flare of a compact source and an arbitrary observer, its scattered light with a given time delay since the moment of the flare is associated with the matter located on the surface of an ellipsoid of rotation. The source and the observer are at the foci of the ellipsoid. Furthermore, in close vicinity of the source, the ellipsoid can be approximated by a paraboloid. Assuming that Sgr A* is the primary source, a detection of the scattered light from a cloud relates the age of the flare and the position of the cloud as

$$t = \frac{\sqrt{x^2 + z^2}}{c} + \frac{z}{c}, \tag{1}$$

where c is the speed of light and x and z are the distances of the cloud from Sgr A* in the sky plane and along the line of sight, respectively.

The degree of polarization P depends on the cosine of the scattering angle μ (in the limit of Thomson scattering) as

$$P = \frac{1 - \mu^2}{1 + \mu^2}, \tag{2}$$

where

$$\mu = -\frac{z}{\sqrt{x^2 + z^2}}. \tag{3}$$

Thus, knowing P, one can reconstruct the 3D position of illuminated clouds. For instance, for $x = 25\,\mathrm{pc}$ and $\theta = 137°$, $z \approx 26\,\mathrm{pc}$, i.e. the illuminated clouds

are further away from us than Sgr A* by this distance. Combining the above three equations, one can explicitly relate the delay time t and the measured degree of polarization P

$$t = \frac{x}{c} \times \left[\left(\frac{1+P}{2P} \right)^{1/2} \pm \left(\frac{1-P}{2P} \right)^{1/2} \right]. \tag{4}$$

This expression was used to estimate the age of the flare.

The determination of the flare luminosity is notoriously difficult, since it depends not only on the distance of the cloud from Sgr A*, but also on the density of the cloud gas and the duration of the flare. One can partly circumvent this problem by using the maximal possible albedo of a molecular cloud [36] to convert the observed X-ray surface brightness into a lower limit on the luminosity

$$L_{4-8,\mathrm{min}} = \frac{I_{4-8}}{\eta_{\mathrm{max}}} 4\pi D_{\mathrm{sc}}^2 \approx 8 \times 10^{37} \,\mathrm{erg\,s^{-1}}, \tag{5}$$

where $I_{4-8} = 4.6 \times 10^{-13} \,\mathrm{erg\,s^{-1}\,cm^{-2}\,arcmin^{-2}} = 5.4 \times 10^{-6} \,\mathrm{erg\,s^{-1}\,cm^{-2}\,sr^{-1}}$ is the observed flux from the studied region [27], $\eta_{\mathrm{max}} \approx 10^{-2}$ is the maximal albedo, and $D_{\mathrm{sc}} = \sqrt{x^2 + z^2} \approx 36\,\mathrm{pc}$ is the distance between Sgr A* and the clouds. Conversion of $L_{4-8,\mathrm{min}}$ to a broader 1–100 keV band assuming a power-law spectrum with the photon index of 2.0 (the value typically measured for the Sgr A GMCs [42]), yields $L_{1-100,\mathrm{min}} \approx 6 \times 10^{38} \,\mathrm{erg\,s^{-1}}$. If the optical depth or, equivalently, the hydrogen column density of illuminated clouds is known, one can use the real albedo in the above equation, driving the minimum luminosity up. Similarly, if only a fraction of the area of the studied region is covered by illuminated clouds, the true luminosity will be higher. For instance, focusing on individual bright clouds, drives this estimate up by an order of magnitude to the level of a few $10^{39} \,\mathrm{erg\,s^{-1}}$ [36], and this is still a lower limit.

However, there is no easy way of placing an upper limit on the source luminosity (for a short flare) without additional explicit assumptions on the gas density and the duration of the flare. For instance, an hour-long flare with a luminosity of $\sim 10^{44}\mathrm{erg\,s^{-1}}$ could be consistent with the data.

Finally, we note that the above derivation assumes that all visible reflection emission is due to a single flare. If Sgr A* produced multiple flares over the past several hundred years [43,44] then the fluxes and polarization will be affected. Longer IXPE observations should be able to test this scenario by providing a polarization measurement of individual GMCs.

References

[27] Ildar Khabibullin, Eugene Churazov, and Rashid Sunyaev. SRG/eROSITA view of X-ray reflection in the Central Molecular Zone: a snapshot in September-October 2019. Monthly Notices of the Royal Astronomical Society, 509(4):6068–6076, February 2022.

[28] Martin C. Weisskopf and et al. The Imaging X-Ray Polarimetry Explorer (IXPE): Pre-Launch. Journal of Astronomical Telescopes, Instruments, and Systems, 8(2):026002, April 2022.

[29] Riccardo Ferrazzoli and et al. In-flight calibration system of imaging x-ray polarimetry explorer. Journal of Astronomical Telescopes, Instruments, and Systems, 6:048002, October 2020.

[30] John Rankin and et al. An Algorithm to Calibrate and Correct the Response to Unpolarized Radiation of the X-Ray Polarimeter Onboard IXPE. Astronomical Journal, 163(2):39, February 2022.

[31] F. Kislat, B. Clark, M. Beilicke, and H. Krawczynski. Analyzing the data from X-ray polarimeters with Stokes parameters. Astroparticle Physics, 68:45–51, August 2015.

[32] A. Di Marco and et al. The ixpe x-ray observatory background. In preparation, 2021.

[33] Luca Baldini and et al. ixpeobssim: A simulation and analysis framework for the imaging X-ray polarimetry explorer. SoftwareX, 19:101194, July 2022.

[34] Fabio Muleri and et al. Performance of the Gas Pixel Detector: an x-ray imaging polarimeter for upcoming missions of astrophysics. In Jan-Willem A. den Herder, Tadayuki Takahashi, and Marshall Bautz, editors, Space Telescopes and Instrumentation 2016: Ultraviolet to Gamma Ray, volume 9905 of Society of Photo-Optical Instrumentation Engineers (SPIE) Conference Series, page 99054G, July 2016.

[35] A. Vikhlinin and et al. Chandra Cluster Cosmology Project. II. Samples and X-Ray Data Reduction. Astrophysical Journal, 692(2):1033–1059, February 2009.

[36] E. Churazov, I. Khabibullin, G. Ponti, and R. Sunyaev. Polarization and long-term variability of Sgr A* X-ray echo. Monthly Notices of the Royal Astronomical Society, 468(1):165–179, June 2017.

[37] M. Revnivtsev and et al. Discrete sources as the origin of the Galactic X-ray ridge emission. Nature, 458(7242):1142–1144, April 2009.

[38] Takayuki Yuasa, Kazuo Makishima, and Kazuhiro Nakazawa. Broadband Spectral Analysis of the Galactic Ridge X-Ray Emission. Astrophysical Journal, 753(2):129, July 2012.

[39] E. Churazov, R. Sunyaev, and S. Sazonov. Polarization of X-ray emission from the Sgr B2 cloud. Monthly Notices of the Royal Astronomical Society, 330(4):817–820, March 2002.

[40] F. Marin, V. Karas, D. Kunneriath, and F. Muleri. Prospects of 3D mapping of the Galactic Centre clouds with X-ray polarimetry. Monthly Notices of the Royal Astronomical Society, 441(4):3170–3176, July 2014.

[41] J. C. Kapteyn. On the motion of Nebulae in vicinity of Nova Persei. Popular Astronomy, 10:124–127, March 1902.

[42] G. Ponti, R. Terrier, A. Goldwurm, G. Belanger, and G. Trap. Discovery of a Superluminal Fe K Echo at the Galactic Center: The Glorious Past of Sgr A* Preserved by Molecular Clouds. Astrophysical Journal, 714(1):732–747, May 2010.

[43] M. Clavel and et al.. Echoes of multiple outbursts of Sagittarius A* revealed by Chandra. Astronomy and Astrophysics, 558:A32, October 2013.

[44] D. Chuard and et al. Glimpses of the past activity of Sgr A* inferred from X-ray echoes in Sgr C. Astronomy and Astrophysics, 610:A34, February 2018.

[45] L. Sidoli and S. Mereghetti. The X-ray diffuse emission from the Galactic Center. Astronomy and Astrophysics, 349:L49–L52, September 1999.

[46] L. Di Gesu and et al. Prospects for IXPE and eXTP polarimetric archaeology of the reflection nebulae in the Galactic center. Astronomy and Astrophysics, 643:A52, November 2020.